Supporting Information

Water-promoted selective photocatalytic methane oxidation for methanol production

Peng Zhou,[†] Songtao Tang,[†] Zhengwei Ye, [†] Ishtiaque Ahmed Navid, [†] Yixin Xiao, [†] Kai Sun[‡] & Zetian Mi[†]*

[†]Department of Electrical Engineering and Computer Science, University of Michigan, Ann Arbor, MI 48109

[‡]Department of Materials Science and Engineering, University of Michigan, 2300 Hayward Street, Ann Arbor, Michigan 48109, United States

Methods

Synthesis of *p*-type InGaN nanowires. *p*-type InGaN nanowires were grown on a 3-inch silicon wafer by PAMBE technology.[1, 2] Silicon wafer was first cleaned with acetone and 10% buffered hydrofluoric acid. Then the residual oxide on silicon wafer was removed by an in-situ annealing at ~787 °C in the reaction chamber before growth. The InGaN NWs were spontaneously grown on silicon wafer under nitrogen-rich conditions. Ga, In and Mg fluxes were controlled by using thermal effusion cells, while nitrogen radicals were produced from a radio-frequency nitrogen plasma source. Multi-stack InGaN/GaN layers were grown on a GaN layer and finally terminated by a GaN capping layer. A nitrogen flow rate of 1.0 sccm and a forward plasma power of ~350 W were used in the growth process.

Cocatalyst loading. AgNPs were loaded on InGaN nanowires by a typical photoreduction process. In a detailed process, a 0.8 cm × 0.8 cm photocatalyst wafer was stabilized on a Teflon holder which was put on the bottom of one 390 mL Pyrex chamber containing 50 mL of 20vol% methanol aqueous solution. Then 10 μL of 0.2 mol L^{-1} $AgNO_3$ (Sigma-Aldrich) was added into the chamber. The chamber equipped with a vacuum-tight quartz lid and a vacuum-tight plastic ring was evacuated before photoreduction. After that, the chamber was irradiated for 20 mins under a 300 W Xe lamp (Cermax, PE300BUV). Finally, the photocatalyst wafer was washed by deionized water and dried at 150 °C in argon atmosphere before photocatalytic methane oxidation.

Characterization. The X-ray diffraction (XRD) pattern of photocatalyst wafer was obtained on a Rigaku X-ray diffractometer equipped with Cu Kα radiation working at the accelerating voltage of 40 kV, the current of 80 mA and the scanning rate of 0.05^{o} 2θ s^{-1}. The microcosmic morphology of samples was examined by a Hitachi SU8000 field emission scanning electron microscopy (FESEM) at an acceleration voltage of 10 kV. The atomic-scale structures of as-prepared samples were analyzed on a double spherical aberration corrected transmission electron microscopy (JEOL 3100R05) with a 300 kV accelerating voltage which generated the high-resolution transmission electron microscopy (HRTEM) and high-angle annular dark field scanning transmission electron microscopy (HAADF-STEM) images. PL measurements were taken with a HORIBA iHR550 spectrometer and an excimer excitation source of 193 nm at a repetition rate of 200Hz.

Photocatalytic methane oxidation. Photocatalytic methane oxidation was performed in 390 mL Pyrex chamber under a 300 Xe lamp (**Figure S1**). The as-prepared 0.8 cm × 0.8 cm photocatalyst wafer was put on the bottom of reaction chamber. The intensity of concentrated light on the photocatalyst wafer was measured to be 5,000 mW cm^{-2} by a thermopile detector (919P, Newport Corporation). 5 mL deionized water was added onto the bottom of chamber. Then feed gas consisting of methane and oxygen with different ratios was introduced to the chamber at atmosphere pressure. The surface temperature of sample was measured by one OMEGA RDXL4SD thermometer equipped with a thermocouple. During reaction, the surface temperature of photocatalyst wafer was determined to be ~170 °C. The gas and liquid products in chamber was manually sampled each 4 hours by using a syringe and analyzed in a gas chromatograph (Shimadzu GC-8A) equipped with two flame ionization detectors. It should be noted that one flame ionization detector was equipped with a methanizer for identifying and quantifying the carbon-based products, including ethane, CO, methanol and CO_2. The TOF for methanol was calculated by the following formula:

TOF = Methanol production amount (mmol) ÷ photocatalyst amount (mmol) ÷ Time (hour)

The mass density of Ga(In)N was 6.15 g cm^{-3}. The amount of photocatalyst on 0.64 cm^2 silicon wafer used in the photocatalytic methane reforming was calculated to be 5.64 μmol (or 0.47 mg).

***In-situ* DRIFTS.** The *In-situ* DRIFTS of photocatalytic methane oxidation on the as-prepared samples was performed on an INVENIO-R Fourier transform infrared spectrometer equipped with a mercury cadmium

telluride (MCT) detector. The DRIFTS system consisted of a praying mantis diffuse reflectance accessory and a reaction cell equipped with a heater (Harrick Scientific). Photocatalyst wafer was put in a sample cup inside the reaction cell. A cover dome contained three windows: one made of quartz permitted the transmission of UV-light beam during *in situ* reactions and two (ZnSe) for the entry and exit of detection infrared beam. Before IR measurement, the samples were firstly pretreated at 300 ^{o}C for 30 min under Ar flow (20 sccm) to clear catalyst surface. After that, the samples were cooled down to 170 ^{o}C which was the same as the test temperature under 300 W Xe lamp. Then the sample was flushed by the methane and oxygen mixture with a certain ratio at the total flow rate of 15 sccm. Meanwhile, the water vapor was introduced into the reaction cell by treating the methane and oxygen mixture through a gas scrubber containing deionized water. A 365 nm LED lamp with a light intensity of 200 mW cm^{-2} was used as the light source to photoexcite the sample. During photocatalytic methane oxidation, the corresponding IR spectra were collected and converted to Kubelka-Munk unit using Omnic™ software.

Theoretical Simulation. The mechanism of photocatalytic methane oxidation on as-prepared samples was studied by the Vienna Ab-initio Simulation Package (VASP). The revised Perdew-Burke-Ernzerh functional of (RPBE) of the generalized gradient approximation (GGA) was used in the calculation of free energy. The interaction between valence electrons and ionic core was described by the PAW pseudo-potential. The InGaN surface was simulated by its typical stable (110) facet which consists of the 3 × 3 supercell with four In/Ga-N layers. It should be noted that the ratio of In and Ga was 1:3 in slab layer according to the experimental PL result. The Ag nanoparticle on InGaN surface was simulated by one Ag cluster (31 atoms) with the diameter of ~1 nm. The convergence threshold of 1.0×10^{-4} eV Å^{-1} and the cutoff of 400 eV were used in the geometry optimization at Gamma point. After geometry optimization, the projected density of states (PDOS) and charge density difference mappings were calculated with Monkhorst-Pack k-point mesh of 2 × 2 × 1, the cutoff of 400 eV and energy convergence threshold of 1.0×10^{-5} eV.

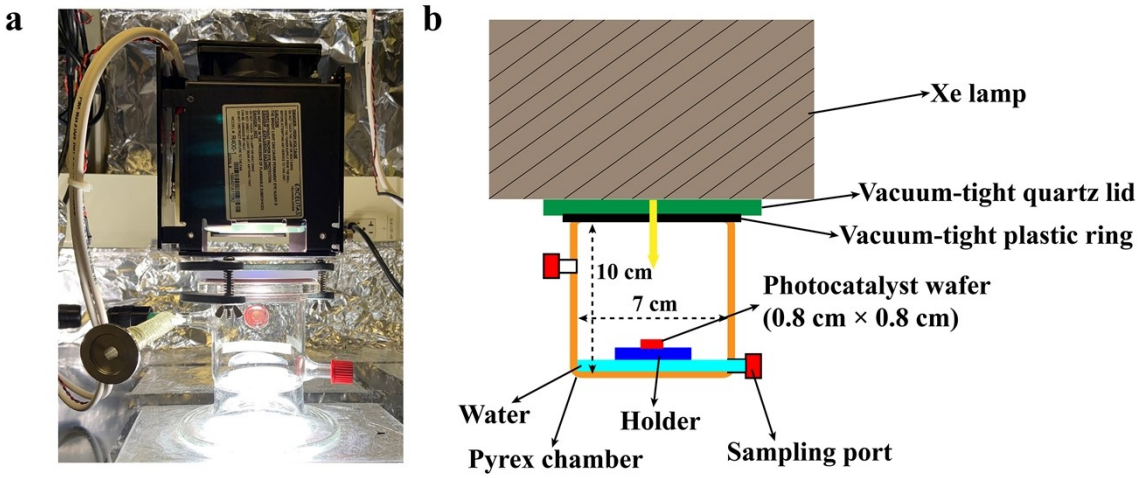

Fig. S1 Reaction system for photocatalytic methane oxidation. **(a)** Image and **(b)** schematic illustration of reaction system.

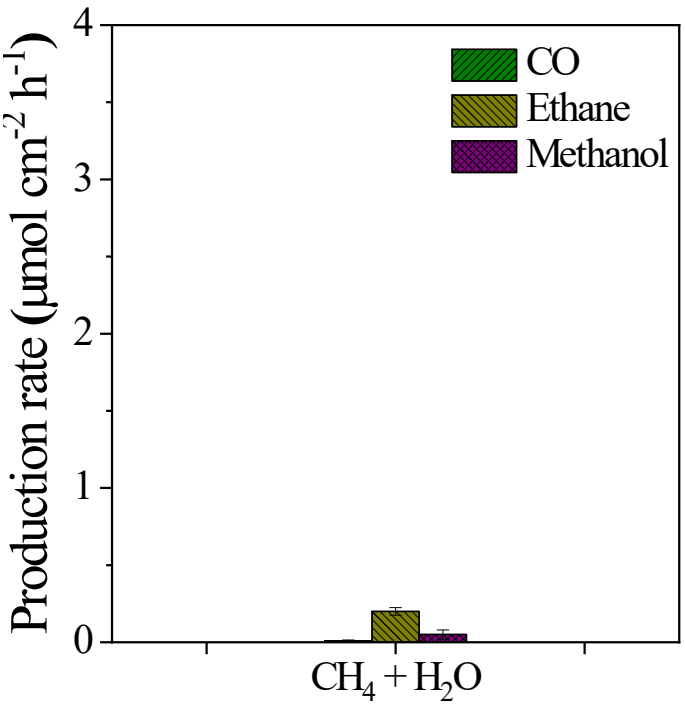

Fig. S2 Photocatalytic methanol production on AgNP-InGaN nanowires without oxygen.

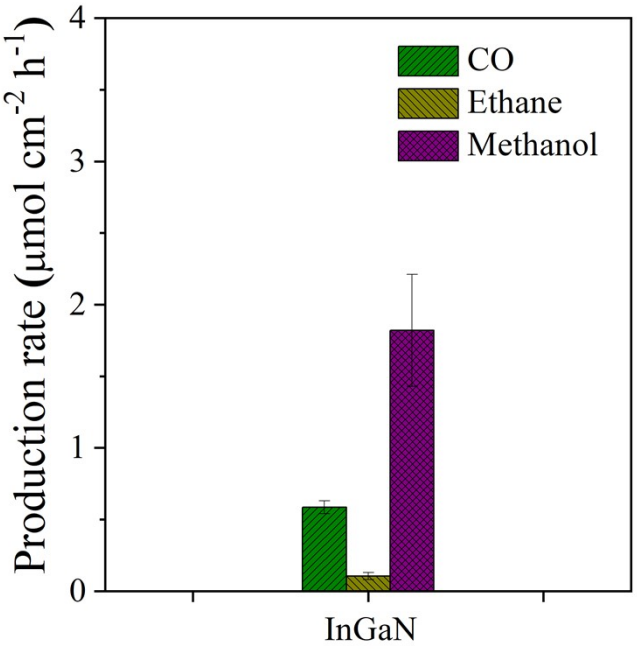

Fig. S3 Photocatalytic methanol production on pristine InGaN nanowires.

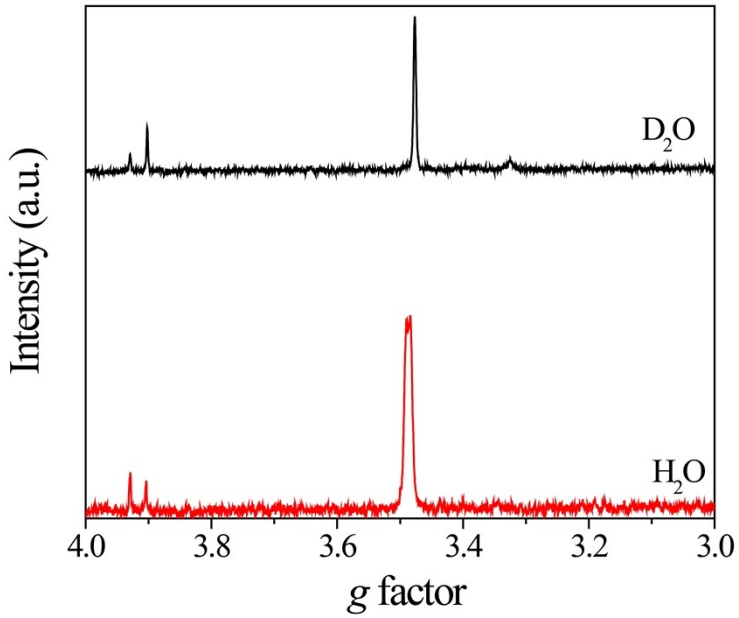

Fig. S4 NMR spectra of methanol produced on AgNP-InGaN nanowires with H_2O or D_2O.

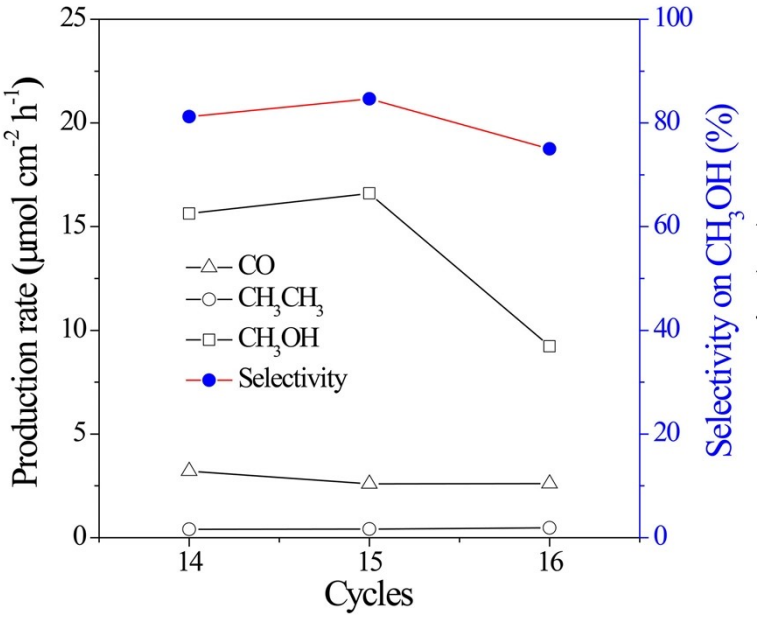

Fig. S5 Activity of Ag/InGaN after 13 cycles.

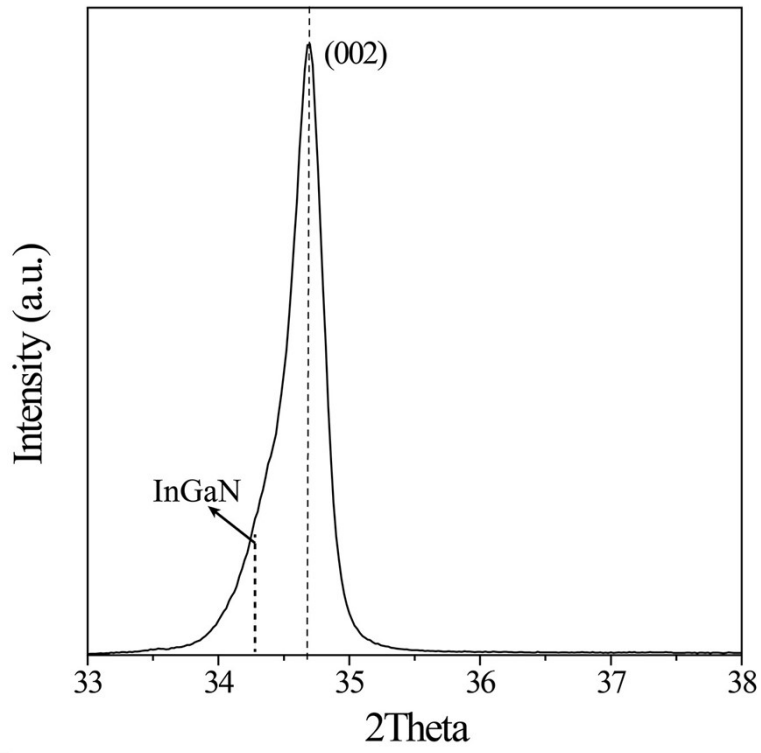

Fig. S6 XRD pattern of Ag/InGaN nanowires after 16 cycles.

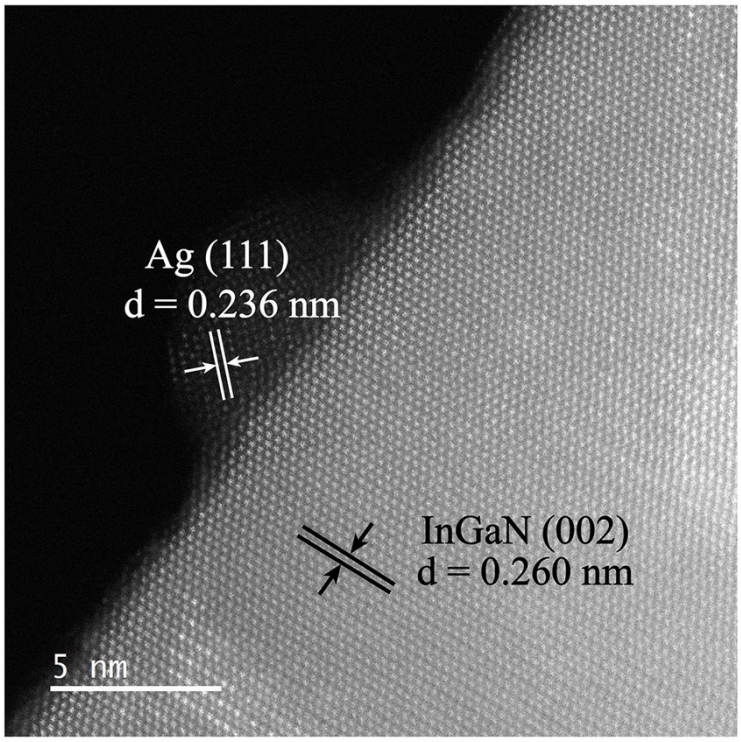

Fig. S7 HAADF-STEM of Ag/InGaN nanowires after 16 cycles.

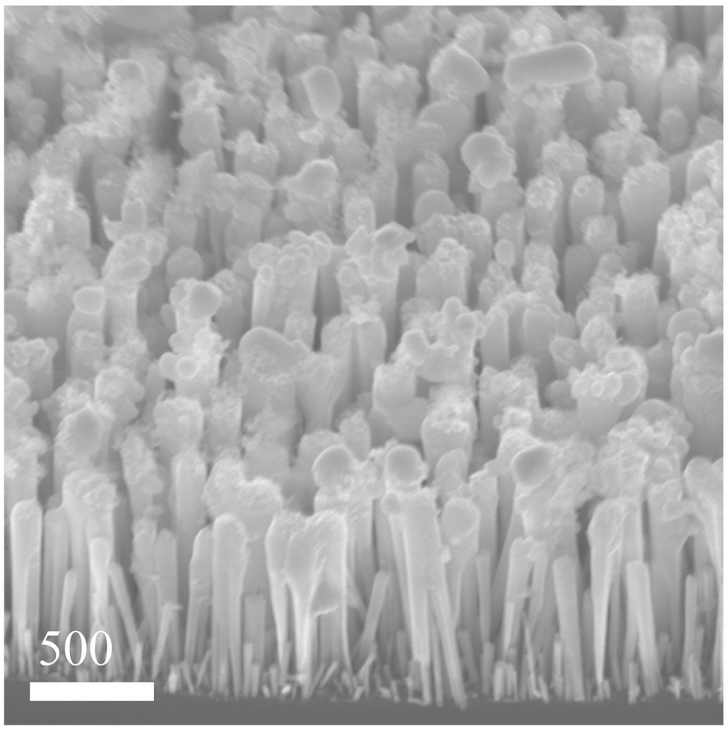

Fig. S8 FESEM images of Ag/InGaN nanowires after 16 cycles.

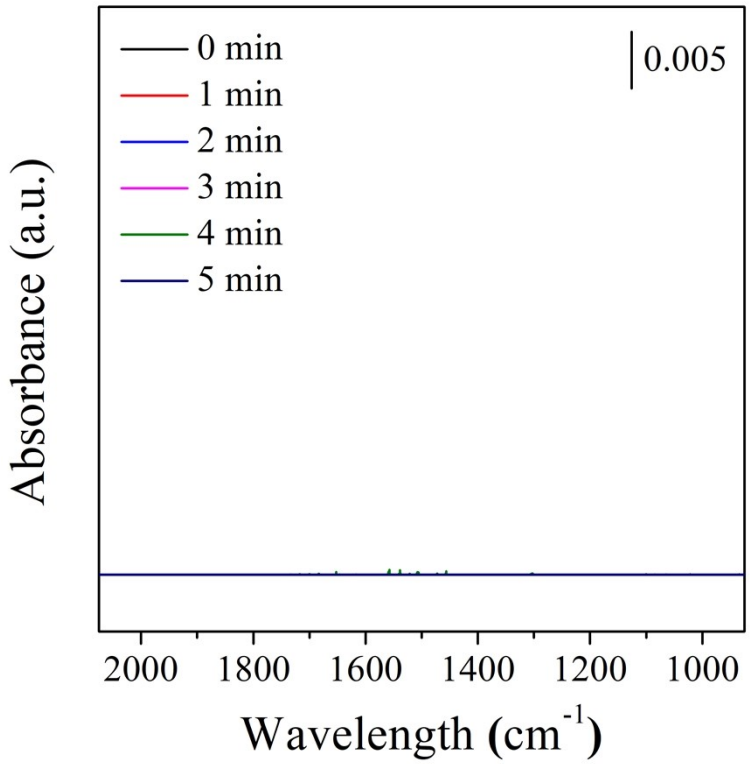

Fig. S9 IR spectrum of Ag/InGaN in the presence of CH_4, O_2 and H_2O under dark.

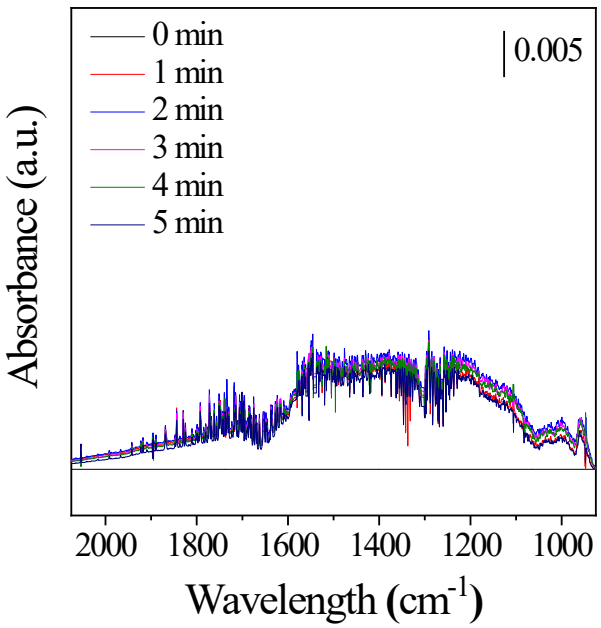

Fig. S10 IR spectrum of pristine InGaN in the presence of CH_4, O_2 and H_2O under irradiation.

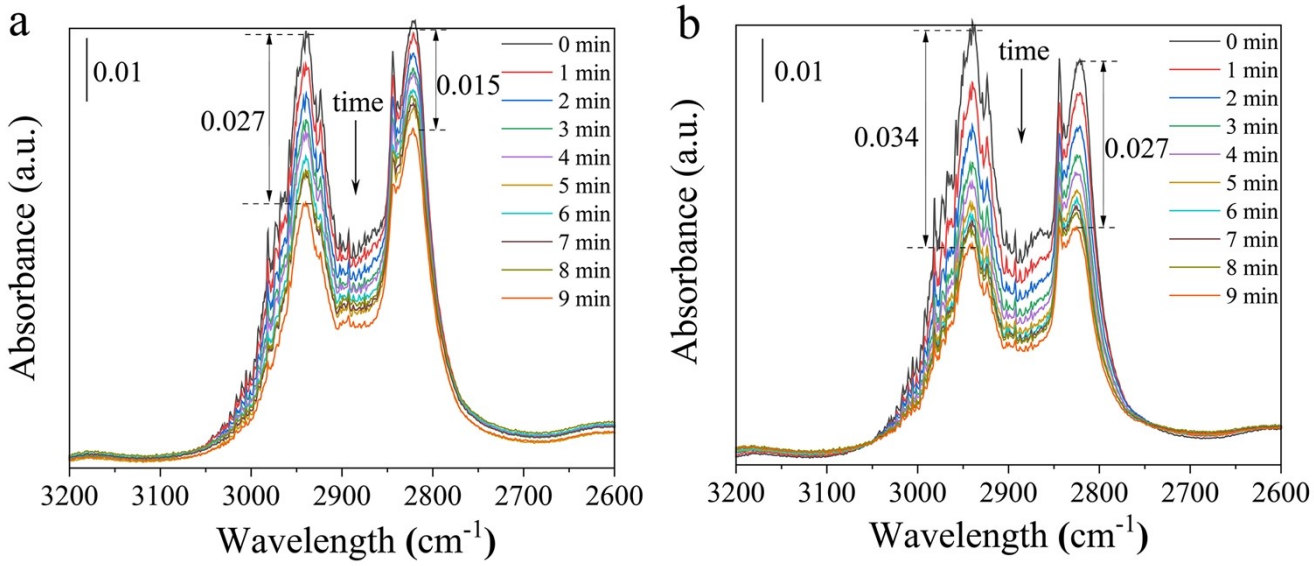

Fig. S11 IR spectrum of methanol desorption on Ag/InGaN (a) without and (b) with water. Ag/InGaN was firstly pretreated before methanol adsorption and desorption measurement. The pretreatment method was same to the above in-situ IR measurement. After pretreatment, the methanol was introduced onto the surface of Ag/InGaN by an Ar carrier at a flow rate of 15 sccm through a gas scrubber containing methanol. After adsorption equilibrium, the purge gas consisting of pure Ar was used to desorb methanol from Ag/InGaN. During desorption process, the corresponding IR spectra were collected. For the water-promoted methanol desorption, the purge gas consisting of Ar and water vapor was used. The IR peaks at 2940 cm^{-1} and 2825 cm^{-1} are assigned to the O-H and C-H bonds, respectively.

Table S1. State-of-the-art photocatalytic systems for reforming methane into methanol.

Photocatalysts	Cocatalysts	Rate (mmol g^{-1} h^{-1})	Stability (hours)	Year [Ref.]
p-InGaN	Ag	45.5	52	This work
ZnO	Pd	6.1	10	2019[3]
TiO_2	FeO_x	0.35	11	2018[4]
TiO_2	Ag	4.8	8	2021[5]
g-C_3N_4	Cu	0.11	2	2019[6]
ZnO	Co_3O_4	0.36	5	2022[7]
ZnO/Fe_2O_3		0.18	30	2022[8]
In_2O_3	Pd atom	0.10	15	2022[9]
PMOF	RuFe(OH)	8.81	120	2022[10]
bismuth vanadate		6.8	7	2021[11]
UiO-66(2.5TFA)-Fe		0.26	1	2021[12]

1. M. G. Kibria, H. P. T. Nguyen, K. Cui, S. Zhao, D. Liu, H. Guo, M. L. Trudeau, S. Paradis, A.-R. Hakima and Z. Mi, *Acs Nano*, 2013, **7**, 7886-7893.
2. M. G. Kibria and Z. Mi, *J. Mater. Chem. A*, 2016, **4**, 2801-2820.
3. H. Song, X. Meng, S. Wang, W. Zhou, X. Wang, T. Kako and J. Ye, *J. Am. Chem. Soc.*, 2019, **141**, 20507-20515.
4. J. J. Xie, R. X. Jin, A. Li, Y. P. Bi, Q. S. Ruan, Y. C. Deng, Y. J. Zhang, S. Y. Yao, G. Sankar, D. Ma and J. W. Tang, *Nat. Catal.*, 2018, **1**, 889-896.
5. N. Feng, H. Lin, H. Song, L. Yang, D. Tang, F. Deng and J. Ye, *Nat. Commun.*, 2021, **12**, 4652.
6. Y. Y. Zhou, L. Zhang and W. Z. Wang, *Nat. Commun.*, 2019, **10**.
7. Z. Xiao, J. Shen, J. Zhang, D. Li, Y. Li, X. Wang and Z. Zhang, *J. Catal.*, 2022, **413**, 20-30.
8. K. Zheng, Y. Wu, J. Zhu, M. Wu, X. Jiao, L. Li, S. Wang, M. Fan, J. Hu, W. Yan, J. Zhu, Y. Sun and Y. Xie, *J. Am. Chem. Soc.*, 2022, **144**, 12357-12366.
9. L. Luo, L. Fu, H. Liu, Y. Xu, J. Xing, C.-R. Chang, D.-Y. Yang and J. Tang, *Nat. Commun.*, 2022, **13**, 2930.
10. B. An, Z. Li, Z. Wang, X. Zeng, X. Han, Y. Cheng, A. M. Sheveleva, Z. Zhang, F. Tuna, E. J. L. McInnes, M. D. Frogley, A. J. Ramirez-Cuesta, L. S. Natrajan, C. Wang, W. Lin, S. Yang and M. Schröder, *Nat. Mater.*, 2022, **21**, 932-938.
11. Y. Fan, W. Zhou, X. Qiu, H. Li, Y. Jiang, Z. Sun, D. Han, L. Niu and Z. Tang, *Nat. Sustain.*, 2021, **4**, 509-515.
12. W. Zhao, Y. Shi, Y. Jiang, X. Zhang, C. Long, P. An, Y. Zhu, S. Shao, Z. Yan, G. Li and Z. Tang, *Angew. Chem. Int. Ed.*, 2021, **60**, 5811-5815.